Journal of
Synchrotron
Radiation

ISSN 0909-0495

Received 8 March 2010
Accepted 26 May 2010

Carbon *K*-edge spectra of carbonate minerals

Jay A. Brandes,[a]* Sue Wirick[b] and Chris Jacobsen[b]

[a]Skidaway Institute of Oceanography, 10 Ocean Science Circle, Savannah, GA 31411, USA, and [b]Department of Physics and Astronomy, SUNY-Stony Brook, Stony Brook, NY 11794, USA. E-mail: jay.brandes@skio.usg.edu

Carbon *K*-edge X-ray spectroscopy has been applied to the study of a wide range of organic samples, from polymers and coals to interstellar dust particles. Identification of carbonaceous materials within these samples is accomplished by the pattern of resonances in the 280–320 eV energy region. Carbonate minerals are often encountered in the study of natural samples, and have been identified by a distinctive resonance at 290.3 eV. Here C *K*-edge and Ca *L*-edge spectra from a range of carbonate minerals are presented. Although all carbonates exhibit a sharp 290 eV resonance, both the precise position of this resonance and the positions of other resonances vary among minerals. The relative strengths of the different carbonate resonances also vary with crystal orientation to the linearly polarized X-ray beam. Intriguingly, several carbonate minerals also exhibit a strong 288.6 eV resonance, consistent with the position of a carbonyl resonance rather than carbonate. Calcite and aragonite, although indistinguishable spectrally at the C *K*-edge, exhibited significantly different spectra at the Ca *L*-edge. The distinctive spectral fingerprints of carbonates provide an identification tool, allowing for the examination of such processes as carbon sequestration in minerals, Mn substitution in marine calcium carbonates (dolomitization) and serpentinization of basalts.

Keywords: carbon; XANES; spectroscopy; carbonate minerals; identification; orientation effects; calcium *L*-edge XANES; sequestration.

1. Introduction

Soft X-ray spectromicroscopy of carbon and other light elements has found an increasing role in the analysis of man-made materials, terrestrial soils and sediments, biofilms, meteorites and extraterrestrial dust (Bluhm *et al.*, 2006; Cody *et al.*, 2008; Brandes *et al.*, 2004; Lehmann *et al.*, 2008; Flynn *et al.*, 2003). Its advantages over methods such as transmission electron microscopy (TEM) and energy electron-loss spectroscopy lie in the lower probability of radiation damage (Hitchcock *et al.*, 2008) and in the ability of many microscopes to handle samples in aqueous or other simulated *in situ* conditions (Kemner *et al.*, 2004). Thus, the combination of imaging and spectral collection (termed spectromicroscopy) (Ade *et al.*, 1990; Hitchcock, 2001), whether over a region using multiple images (Jacobsen *et al.*, 2000) or at points or along lines (Ade *et al.*, 2003), can provide unique information on the speciation and bonding environment of most elements.

Although most studies using C *K*-edge spectroscopy have examined organic or polymeric materials, the potential exists for the use of this method in the study of inorganic carbonate minerals. Many studies of organic matter in soils, sediments and other environmental samples (Lepot *et al.*, 2008; Politi *et al.*, 2008; Obst *et al.*, 2009; Hitchcock *et al.*, 2008; Benzerara, Miller *et al.*, 2006; Flynn *et al.*, 2004*a*; Takahama *et al.*, 2007; Lemelle *et al.*, 2004; Lawrence *et al.*, 2003) mention the presence of carbonates, which are easily distinguished from other C forms by the presence of a strong 290 eV resonance. These carbonates are generally assigned to be either calcite or aragonite, although occasionally other polymorphs of $CaCO_3$ are noted. However, the range of spectra assigned to either mineral is quite broad, from those with only one central peak at 290 eV to those exhibiting a variety of higher-energy resonances (Lawrence *et al.*, 2003; Zhou *et al.*, 2008; Benzerara, Menguy *et al.*, 2006). Other carbonate minerals, such as those with Fe, Mn and Mg cations, may be present in samples but there is often no simple method to verify their presence without employing a higher-energy beamline capable of reaching heavier elemental absorption edges. No single study has provided a systematic examination of carbonate mineral C *K*-edge spectra. We present here a library of common carbonate X-ray absorption near-edge structure (XANES) spectra that can be used to fingerprint these minerals in samples.

2. Methods

Minerals were purchased from reputable dealers, and only large (> 5 mm diameter) identifiable crystals were selected for

analysis. Minerals were identified by physical characteristics (crystal shape, color, luster, susceptibility to acid dissolution) prior to analysis. Most samples were sectioned using a Leica Ultramicrotome to a thickness of approximately 150 nm. Small (~1 mm) mineral pieces were embedded in Epofix epoxy or embedded in S^o prior to sectioning. All sections were placed on SiO-supported copper TEM grids prior to analysis. Also, an additional set of mineral samples was analyzed without sectioning, by grinding into a fine power, dispersing onto a droplet of double-distilled water and final placement onto a SiO-supported grid by direct contact of the grid on the water surface. The percent organic carbon content of each mineral was also determined by elemental analysis after acid fumigation to remove carbonates (Hedges & Stern, 1984). No mineral exhibited an organic content greater than 1% except for aragonite, which was less than 5%.

Images and stacks of images (Jacobsen *et al.*, 2000) were collected using the scanning transmission X-ray microscope (STXM) located on beamline X1-A1 (outboard branch) at the National Synchrotron Light Source, Brookhaven National Laboratory (Winn *et al.*, 2000). Complete details of the design, operation and capabilities of the microscope are described by Feser *et al.* (2000, 2001). Briefly, synchrotron-generated monochromatic X-ray radiation is focused by a Fresnel zone plate onto a sample with a focal point spot size defined by the outer-most zone spacing of the zone plate. For this work that distance was 35 nm. Samples are mounted perpendicular to the beam. The sample stage is moved in the *xy*-plane using a piezo stage so that an X-ray transmission absorption map is collected of the sample. Spectra can be obtained either *via* direct analysis at one point, recording absorbance changes with changes in X-ray energy, or by collecting a series of images over different energies and combining them to form an *x* by *y* by eV data 'stack'. Typical stack sizes were 100 × 100 pixels of 0.1 μm size. The energy resolution of the monochromator is 0.1 eV. All samples were examined using the 'stack' method, and each analysis included a minimum of 10–20 micro-crystalline powder particles. Principle component analysis was used to orthogonalize and noise-filter the spectromicroscopy stack data (Osanna *et al.*, 1996). Cluster analysis was then used to classify pixels according to spectral similarity, and to extract representative cluster-averaged spectra with good signal-to-noise ratios (Lerotic *et al.*, 2004, 2005). This method allowed us to select regions of optimal thickness (especially in powder samples) and similar orientation.

Energy values were calibrated using CO_2 and its known absorption energies just prior to analyses (Ma, 1991). The steps per eV and zero-order position of the spherical-grating monochromator used at the X1A1 beamline is determined by measuring peak positions of CO_2, N_2 and O_2. Energy stability during repeated scans was within 0.1 eV, the resolution of the monochromator. Calcium peak positions were also compared with calcium *L*-edge spectra of calcite collected at beamline 5.32 at the Advanced Light Source in Berkeley and found to be in agreement. Peak positions were determined using the *IDL* software package. For the carbonate minerals, spectral peak positions, intensities and widths were determined using the *ATHENA* software package (Ravel & Newville, 2005) and represent iteratively determined 'best fits' of the primary peaks based upon minimization of the χ^2 value reported by the software.

Table 1
X-ray energies (in eV) for primary absorption peaks of different carbonate minerals in the carbon *K*-edge XANES region.

br = broad.

Mineral	Formula	Primary peak	Secondary peaks
Calcite	$CaCO_3$	290.1	295.2, 298.0, 301.3
Aragonite	$CaCO_3$	290.2	295.2, 298.0, 301.3
Dolomite	$(Ca,Mg)CO_3$	290.2	295.9, 298.0, 301.1
Ankerite	$Ca(Fe,Mg,Mn)CO_3$	290.1	297.6, 302 br
Magnesite	$MgCO_3$	290.2	298.1, 300.25
Rhodochrosite	$MnCO_3$	290.2	293.8, 300.8 br
Siderite	$FeCO_3$	290.2	288.6, 300 br
Gaspeite	$(Ni,Mg,Fe)CO_3$	290.1	288.6, 298 br, 300.5 br, 302.5 br,
Spalerocobaltite	$CoCO_3$	290.3	288.6, 295.9, 300.75
Smithsonite	$ZnCO_3$	290.1	288.7, 299.3, 301.8
Strontitanite	$SrCO_3$	290.2	295.2, 300.8 br
Witherite	$BaCO_3$	290.2	288.6, 299.9, 302.3
Cerussite	$PbCO_3$	289.9	291.6, 299.5 br

3. Results

Table 1 and Figs. 1, 2 and 3 summarize the carbon *K*-edge XANES data from the 11 carbonate minerals examined. All minerals exhibited a sharp resonance at 290.2 (±0.1) eV with the exception of lead carbonate, which had a slightly lower resonance at 289.9 eV. However, most species had resonances that provide spectral 'fingerprints' that can be used to differentiate between minerals without using electron microprobes or higher-energy X-ray absorption fine structure (XAFS) measurements. Calcite and aragonite are compositionally identical minerals, differing only in crystal structure; thus it is not surprising that they had essentially identical peak positions (within 0.1 eV) (Table 1) at the carbon *K*-edge. However, the inclusion of Mg in dolomite changed the resulting carbon XANES spectra in notable ways. The 295 eV peak was shifted higher in intensity by 0.6 eV, with a sharper and more isolated peak than found in either calcite or aragonite. The distinct resonance at 298 eV present in pure calcium carbonates was reduced to a shoulder on the main 301 eV peak in dolomite. Interestingly, the dolomite spectra were not a linear combination of $CaCO_3$ and $MgCO_3$ spectra.

Witherite, sphaerocobaltite, siderite and smithsonite all exhibited a well defined pre-edge peak at 288.6 eV in addition to the expected 290.2 eV and higher absorbances. This energy region is normally assigned to carbonyl moieties (Urquhart & Ade, 2002) and has not been previously reported in carbonates. Indeed, the specimen of aragonite used for this study, a coral skeleton sample, has a small 288.5 eV peak associated with organic matter. None of the other minerals examined contained more than 1% organic carbon (non-acid volatile). It is therefore unlikely that organic matter is responsible for the

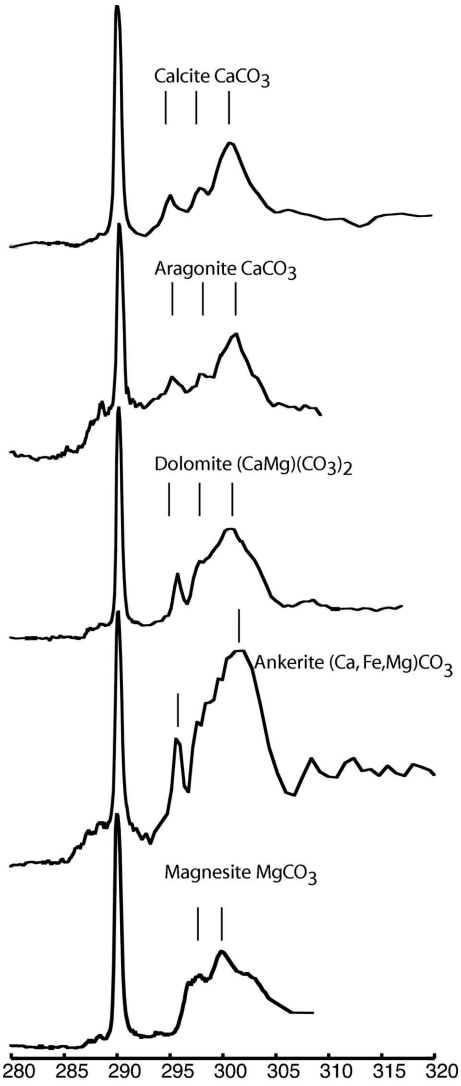

Figure 1
Ca- and Mg-containing carbonate mineral C *K*-edge XANES spectra. The *x* axis is in units of eV and the *y* axis is normalized fluorescence intensity. Vertical lines represent locations of peaks described in Table 1.

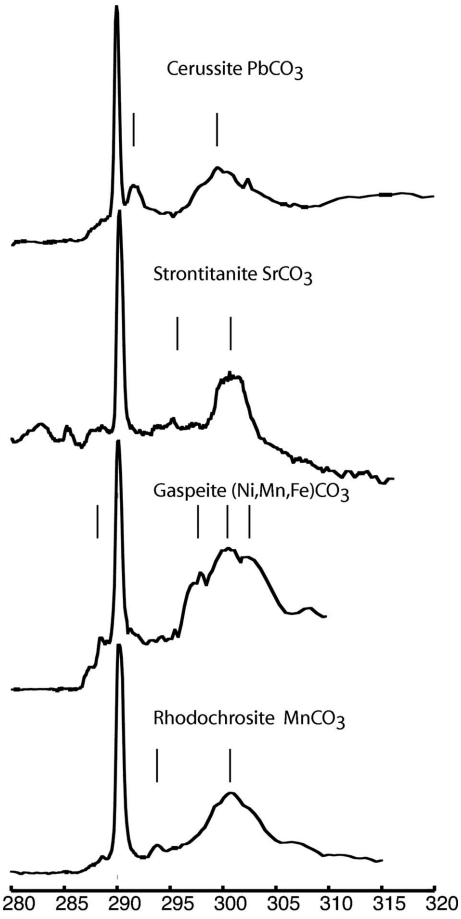

Figure 2
C *K*-edge XANES spectra of Pb, Sr, Mn and transition-metal carbonates. The *x* axis is in units of eV and the *y* axis is normalized fluorescence intensity. Vertical lines represent locations of peaks described in Table 1.

288.6 eV peak in these minerals, especially in witherite. No natural compound, in our experience, exhibits the required molar absorption coefficient to produce the peak observed in witherite at a 1% abundance. The 288.6 eV peak present in Fig. 3 may possibly be attributed to a change in bonding environment (*e.g.* partial reduction) around the carbon atoms in the mineral. Of the four minerals with strong 288.6 eV peaks, witherite ($BaCO_3$) exhibited a significantly stronger peak than the others.

Cerrusite ($PbCO_3$) exhibited a close post-290.2 eV peak at 291.6 eV. Strontitanite also was notable for having a number of small pre-287 eV resonances. These are likely associated with the Sr *M*(II) resonance around 280 eV (Stöhr, 1992) and not with any C resonance.

Calcium *L*-edge spectroscopy has been used to identify carbonate minerals (Obst *et al.*, 2009; Fleet & Liu, 2009; Naftel *et al.*, 2001; Hanhan *et al.*, 2009; Benzerara *et al.*, 2004). Calcium *L*-edge spectra of aragonite and calcite (Table 2, Fig. 4) differed in both peak positions and intensities. Both minerals exhibited strong absorption peaks at 349.5 and 352.7 eV. However, calcite was distinguished by two strong resonances at 348.2 eV and 351.4 eV. Aragonite had much smaller peak resonances at 347.8, 348.4 and 351.8 eV. Ankerite [$(Ca, Fe, Mg)CO_3$] and dolomite both had Ca XANES spectra almost identical to that of calcite. It has been previously noted (Benzerara *et al.*, 2004; Fleet & Liu, 2009) that the Ca XANES is primarily influenced by crystal orientation, trigonal in the cases of calcite, ankerite and dolomite but orthorhombic in the case of aragonite. The presence of $MgCO_3$ layers within dolomite does not appear to influence its Ca XANES significantly.

4. Orientation effects

Owing to the linear polarization of the X-ray beam, the XANES spectra for all but cubic crystals are subject to crystal axes orientation effects. Carbon XANES spectra of carbonates are susceptible to these linearly polarized beam orientation effects (Davis *et al.*, 1993; Zhou *et al.*, 2008). Although samples were not rotated relative to the beam, different crystals within the powders analyzed in this study exhibited

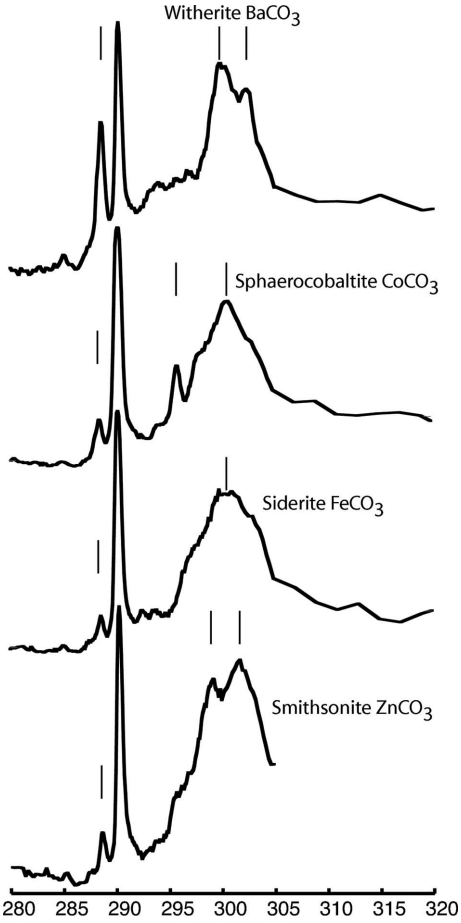

Figure 3
C *K*-edge XANES spectra of carbonates exhibiting significant pre-edge 288.6 eV peaks. The *x* axis is in units of eV and the *y* axis is normalized fluorescence intensity. Vertical lines represent locations of peaks described in Table 1.

different spectra consistent with orientation effects. In general, the orientation effects observed in this study shifted the relative intensity of dominant peaks from predominantly π^* at 290 eV to the higher-energy σ^* resonances (Fig. 5). Carbonate ions, with a trigonal planar shape, will exhibit the strongest π^* resonance when the molecule is 'edge on' to the beam. This phenomenon can make identification of carbonates problematic in organic samples, especially if the σ^* resonances are masked by organic carbon σ^* resonances. In extreme cases the π^* resonance can almost disappear (Davis *et al.*, 1993; Zhou *et al.*, 2008). A similar phenomenon occurs with graphite (Watts & Ade, 2008; Brandes *et al.*, 2008). In most cases the σ^* resonances have proportionally the same relative energies at high and low angle (compare Figs. 1, 2, 3 and 4). This does not appear to be the case for magnesite ($MgCO_3$), where a σ^* resonance at 298 eV becomes proportionally much stronger at high angles relative to the Ca–O molecular plane. Smaller discrepancies between high- and low-angle spectra are found in rhodochrosite ($MnCO_3$) (although some of this may be due to low signal-to-noise spectra on this region) and witherite ($BaCO_3$). Carbonyl moieties are less susceptible to orientation effects, thus the 288.6 eV peaks in $BaCO_3$, $CoCO_3$ and $FeCO_3$ appear to be less diminished than the corresponding 290.1 eV peaks in these minerals at high angle (Fig. 5). It is also possible that these groups are present at different orientations than the carbonate groups, however.

Table 2
X-ray energies (in eV) for primary absorption peaks of different carbonate minerals in the calcium *L*-edge XANES region.

m = minor peak.

Mineral	Formula	Peak positions
Calcite	$CaCO_3$	347.4 m, 348.1, 349.4, 351.3, 352.6
Aragonite	$CaCO_3$	347.4 m, 348.4 m, 348.5 m, 349.4, 351.8 m, 352.6
Dolomite	$(Ca,Mg)CO_3$	347.0 m, 347.5 m, 348.1, 349.3, 351.4, 352.6
Ankerite	$Ca(Fe,Mg,Mn)CO_3$	347.1 m, 348.2, 349.4, 351.4, 352.6

5. Discussion

Carbon *K*-edge XANES has become a powerful tool for the examination of organic matter in soils, sediments, minerals and

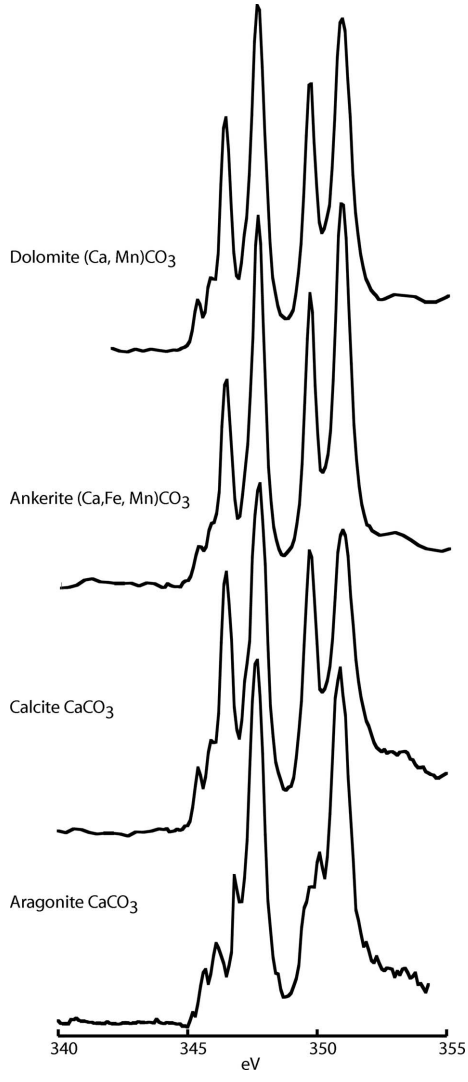

Figure 4
Calcium *L*-edge XANES of aragonite, calcite, ankerite and dolomite. The *x* axis is in units of eV and the *y* axis is normalized fluorescence intensity.

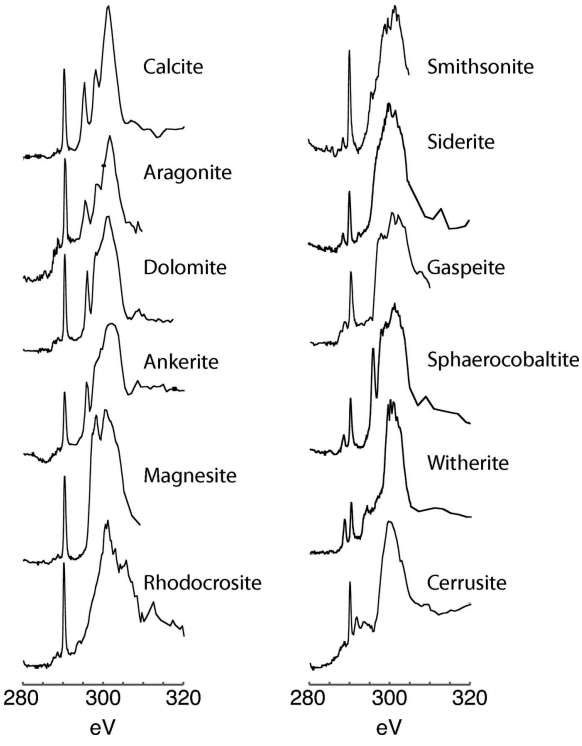

Figure 5
C *K*-edge XANES spectra of mineral carbonates at high apparent beam angle to crystal orientation. The *x* axis is in units of eV and the *y* axis is normalized fluorescence intensity.

aerosols (Brandes *et al.*, 2004; Boyce *et al.*, 2004; Takahama *et al.*, 2007; Lehmann *et al.*, 2009). The primary difficulty in application of this analytical method towards natural samples is the difficulty in spectral interpretation. Even relatively simple systems such as amino and polyamino acids can exhibit startling shifts in C XANES (Gordon *et al.*, 2003). Although easier to interpret than organic spectra, C XANES of minerals also exhibit shifts owing to orientation effects. Within the literature there are several examples of 'carbonate' spectra exhibiting the phenomena shown in our data. Takahama *et al.* (2007) examined a set of aerosol particles collected along a transect in Mexico, and noted several 'carbonate' particles. In at least one case (their Fig. 1*n*) the particle is clearly calcite/aragonite at low angles (owing to high σ^* and low π^* resonances) with a co-existing organic matrix. Metzler *et al.* (2008) examined the influence of nacre (organic $CaCO_3$) forming polypeptides on calcite formation. Their study noted that such molecules appeared to 'disrupt' CO bonds in calcite (owing to the appearance of a 288 eV peak). However, this 288 eV peak was noted to be only present in mineral surface (PEEM) measurements, not in total electron yield measurements that would more closely correspond to the transmission XANES measurements presented here. Their reported σ^* peak positions in calcite of 295, 298 and 301.5 eV correlate well with those we report in Table 1. $CaCO_3$ grown in the presence of polypeptides had significantly weaker σ^* resonances, with the highest resonance shifted to a lower energy.

The influence of intercalcated organic molecules noted by Metzler *et al.* (2008) can also be seen in other examples from the literature. Measurements of 'carbonates' in biofilms (Lawrence *et al.*, 2003) and fossilized microbialites (Benzerara, Menguy *et al.*, 2006; Benzerara, Miller *et al.*, 2006) both show a near absence of 295 and 298 eV peaks and a more square-shaped 300 eV peak. This may be due to a structural effect caused by organic molecules disrupting the crystal lattice of calcite as noted above (Metzler *et al.*, 2008) or orientation effects (Zhou *et al.*, 2008). We did not, however, note this effect in our biogenetically produced (coral) aragonite specimen (Fig. 1).

The presence of a 288.6 eV peak in Zn, Fe, Co and especially Ba carbonates is intriguing (Fig. 3). This peak is generally assigned to carbonyl or carboxylic acid moieties (Urquhart & Ade, 2002; Lehmann *et al.*, 2009) and not to carbonate. As noted above, Metzler *et al.* (2008) noted in their PEEM measurements the presence of a 288 eV peak in their artificially precipitated calcite, but not in their natural (geological specimen) sample, and attributed it to a 'surface disruption of CO bonds'. Since the transmission XANES collected here will tend to dilute any such surface signals, and our Ca carbonate mineral spectra exhibited no such 288 eV peaks (aside from a very small peak in aragonite, likely due to the presence of intermixed organic matter), the data suggest the presence of a significant amount of carbonyl character within these minerals. It is unclear if this phenomenon is the result of incorporation of a high percentage of carbonyl-rich organic matter or the partial reduction of carbonate. The argument against organic matter is the lack of significant 285 (aromatic C) or 288.0 eV (aliphatic) peaks in any of the minerals in Fig. 3. Indeed, to obtain the 288.6 eV peak in $BaCO_3$ one would require significantly more than 10% organic matter content, unless such organic matter were extremely cabonyl-rich. By way of contrast, we measured <5% non-acid volatile organic C in our aragonite sample, and less than 2% in the other mineral samples, by elemental analysis after HCl fumigation (Hedges & Stern, 1984). As the aragonite 288.6 eV peak was an order of magnitude smaller than that found in $BaCO_3$, it appears unlikely that the large 288.6 eV peak in the latter mineral is caused by organic contaminants. However a partial reduction of carbonate or 'disruption' of CO_3^- bonding is also unexplainable, especially in $BaCO_3$ where Ba is unlikely to change oxidation states from +2. However, Isherwood & James (1976) reported results that suggest that C—O bond lengths in carbonate minerals are influenced by the electronegativity of the cation species with the carbonate C—O anion bond length decreasing with increasing cation electronegativity. Skinner *et al.* (1994) reported charge density contour plots for calcite which show the carbonate anion to be a mix of both covalent and ionic charge states. They also reported a degenerative state of hybrid orbitals formed between O 2*p* and C states with some mixing of O 2*s* states. With increasing electronegativity of the cation the carbonate ion may form a more ionic than covalent bond with the cation distorting the carbonate anion such that

resonances from C═O are observed in the carbon near-edge structure.

The high resolution afforded by C-XANES and STXM imaging provides a useful tool for the examination of the formation of carbonates during CO_2 incorporation into minerals. Carbon sequestration into calcium- and magnesium-rich rocks has been proposed as a possible method for reducing atmospheric CO_2 emissions from fossil fuel burning (Oelkers *et al.*, 2008). Especially in the absence of high concentrations of organic matter, the mapping of C-XANES spectra at 40 nm (or less) spatial resolution affords a look into the basic reaction chemistry of this process. Given that the XANES spectra of Ca, Ca–Mn, Mn and Mg carbonates all differ, one can bring to bear principle component analysis and cluster analysis techniques to map reaction extent and mineral composition in samples. Indeed, this has been shown to be quite a useful technique in the study of organic and inorganic matter in biofilms, marine sediments and meteorites (Flynn *et al.*, 2004*b*; Brandes *et al.*, 2004; Jacobsen *et al.*, 2003; Lehmann *et al.*, 2005, 2008; Schumacher *et al.*, 2005; Toner *et al.*, 2005).

Finally, the ability of Ca-XANES to distinguish between aragonite and calcite at STXM resolutions provides an additional check on the composition and alteration of carbonate minerals within sediments, rocks and other heterogeneous samples. As the C *K*-edge and Ca *L*-edge regions lie within 70 eV of each other it is possible on many STXM instruments to collect both sets of spectra on the same region without realigning or otherwise disturbing sample–optics orientation. Using the combination of both elements, one can distinguish between aragonite, calcite and dolomite without having to resort to micro X-ray diffraction or micro X-ray fluorescence techniques.

This material is based upon work supported by the National Science Foundation under grants NSF OCE-0526178 and -0221295. Any opinions, findings and conclusions or recommendations expressed in this material are those of the author(s) and do not necessarily reflect the views of the National Science Foundation. Funding for both the ALS and NSLS is provided by the Department of Energy. The X1A1 STXM is supported by New York State's Science and Technology program.

References

Ade, H., Kilcoyne, A. L. D., Tyliszczak, T., Hitchcock, P., Anderson, E., Harteneck, B., Rightor, E. G., Mitchell, G. E., Hitchcock, A. P. & Warwick, T. (2003). *J. Phys. IV*, **104**, 3–8.

Ade, H., Kirz, J., Hulbert, S. L., Johnson, E., Anderson, E. & Kern, D. (1990). *Appl. Phys. Lett.* **56**, 1841–1843.

Benzerara, K., Menguy, N., Lopez-Garcia, P., Yoon, T. H., Kazmierczak, J., Tyliszczak, T., Guyot, F. & Brown, G. E. (2006). *Proc. Natl. Acad. Sci. USA*, **103**, 9440–9445.

Benzerara, K., Miller, V. M., Barell, G., Kumar, V., Miot, J., Brown, G. E. & Lieske, J. C. (2006). *J. Investig. Med.* **54**, 367–379.

Benzerara, K., Yoon, T. H., Tyliszczak, T., Constantz, B., Spormann, A. M. & Brown, G. E. (2004). *Geobiology*, **2**, 249–259.

Bluhm, H. *et al.* (2006). *J. Electron Spectrosc. Relat. Phenom.* **150**, 86–104.

Boyce, C. K., Zwieniecki, M. A., Cody, G. D., Jacobsen, C., Wirick, S., Knoll, A. H. & Holbrook, N. M. (2004). *Proc. Natl. Acad. Sci. USA*, **101**, 17555–17558.

Brandes, J. A., Cody, G. D., Rumble, D., Haberstroh, P., Wirick, S. & Gelinas, Y. (2008). *Carbon*, **46**, 1424–1434.

Brandes, J. A., Lee, C., Wakeham, S., Peterson, M., Jacobsen, C., Wirick, S. & Cody, G. (2004). *Marine Chem.* **92**, 107–121.

Cody, G. D. *et al.* (2008). *Meteorit. Planet. Sci.* **43**, 353–365.

Davis, R., Walsh, J. F., Muryn, C. A., Thornton, G., Dhanak, V. R. & Prince, K. C. (1993). *Surf. Sci.* **298**, L196–L202.

Feser, M., Beetz, T., Carlucci-Dayton, M. & Jacobsen, C. (2000). *AIP Conf. Proc.* **507**, 367–372.

Feser, M., Beetz, T., Carlucci-Dayton, M. & Jacobsen, C. (2001). *Soft X-ray and EUV Imaging Systems II*, edited by D. A. Tichenor and J. A. Folta, pp. 146–153. Bellingham: Society of Photo-Optical Instrumentation Engineers.

Fleet, M. E. & Liu, X. Y. (2009). *Am. Mineral.* **94**, 1235–1241.

Flynn, G. J., Keller, L. P., Feser, M., Wirick, S. & Jacobsen, C. (2003). *Geochim. Cosmochim. Acta*, **67**, 4791–4806.

Flynn, G. J., Keller, L. P., Jacobsen, C. & Wirick, S. (2004*a*). *Bioastronomy 2002: Life Among the Stars*, pp. 275–280. San Francisco: Astronomical Society of the Pacific.

Flynn, G. J., Keller, L. P., Jacobsen, C. & Wirick, S. (2004*b*). *Space Life Sciences: Steps Toward Origin(s) of Life*, Vol. 33, pp. 57–66. Kidlington: Pergamon-Elsevier Science.

Gordon, M. L., Cooper, G., Morin, C., Araki, T., Turci, C. C., Kaznatcheev, K. & Hitchcock, A. P. (2003). *J. Phys. Chem. A*, **107**, 6144–6159.

Hanhan, S., Smith, A. M., Obst, M. & Hitchcock, A. P. (2009). *J. Electron Spectrosc. Relat. Phenom.* **173**, 44–49.

Hedges, J. I. & Stern, J. H. (1984). *Limnol. Oceanogr.* **29**, 657–663.

Hitchcock, A. P. (2001). *J. Synchrotron Rad.* **8**, 66–71.

Hitchcock, A. P., Dynes, J. J., Johansson, G., Wang, J. & Botton, G. (2008). *Micron*, **39**, 311–319.

Isherwood, B. J. & James, J. A. (1976). *Acta Cryst.* A**32**, 340–341.

Jacobsen, C., Feser, M., Lerotic, M., Vogt, S., Maser, J. & Schafer, T. (2003). *J. Phys. IV*, **104**, 623–626.

Jacobsen, C., Flynn, G., Wirick, S. & Zimba, C. (2000). *J. Microsc.* **197**, 173–184.

Kemner, K. M., Kelly, S. D., Lai, B., Maser, J., O'Loughlin, E. J., Sholto-Douglas, D., Cai, Z. H., Schneegurt, M. A., Kulpa, C. F. & Nealson, K. H. (2004). *Science*, **306**, 686–687.

Lawrence, J. R., Swerhone, G. D. W., Leppard, G. G., Araki, T., Zhang, X., West, M. M. & Hitchcock, A. P. (2003). *Appl. Environ. Microbiol.* **69**, 5543–5554.

Lehmann, J., Brandes, J. A., Jacobsen, C., Solomon, D. & Thieme, J. (2009). *Synchrotron-Based Near-Edge X-ray Spectroscopy of NOM in Soils and Sediments, Biophysico-Chemical Processes Involving Natural Nonliving Organic Matter in Environmental Systems*, edited by N. Senesi, B. Xing and P. M. Huang, pp. 729–782. Hoboken: Wiley.

Lehmann, J., Liang, B. Q., Solomon, D., Lerotic, M., Luizao, F., Kinyangi, J., Schafer, T., Wirick, S. & Jacobsen, C. (2005). *Global Biogeochem. Cycles*, **19**, GB1013.

Lehmann, J., Solomon, D., Kinyangi, J., Dathe, L., Wirick, S. & Jacobsen, C. (2008). *Nat. Geosci.* **1**, 238–242.

Lemelle, L., Salome, M., Fialin, M., Simionovici, A. & Gillet, P. (2004). *Spectrochim. Acta B*, **59**, 1703–1710.

Lepot, K., Benzerara, K., Brown, G. E. & Philippot, P. (2008). *Nat. Geosci.* **1**, 118–121.

Lerotic, M., Jacobsen, C., Gillow, J. B., Francis, A. J., Wirick, S., Vogt, S. & Maser, J. (2005). *J. Electron Spectrosc. Relat. Phenom.* **144**, 1137–1143.

Lerotic, M., Jacobsen, C., Schafer, T. & Vogt, S. (2004). *Ultramicroscopy*, **100**, 35–57.

Ma, Y., Chen, C. T., Meigs, G., Randall, K. & Sette, F. (1991). *Phys. Rev. A*, **44**, 1848–1858.

Metzler, R. A., Kim, I. W., Delak, K., Evans, J. S., Zhou, D., Beniash, E., Wilt, F., Abrecht, M., Chiou, J. W., Guo, J. H., Coppersmith, S. N. & Gilbert, P. (2008). *Langmuir*, **24**, 2680–2687.
Naftel, S. J., Sham, T. K., Yiu, Y. M. & Yates, B. W. (2001). *J. Synchrotron Rad.* **8**, 255–257.
Obst, M., Dynes, J. J., Lawrence, J. R., Swerhone, G. D. W., Benzerara, K., Karunakaran, C., Kaznatcheev, K., Tyliszczak, T. & Hitchcock, A. P. (2009). *Geochim. Cosmochim. Acta*, **73**, 4180–4198.
Oelkers, E. H., Gislason, S. R. & Matter, J. (2008). *Elements*, **4**, 333–337.
Osanna, A., Jacobsen, C., Kalinovsky, A., Kirz, J., Maser, J. & Wang, S. (1996). *Scanning Microsc. Suppl.* **10**, 349–358.
Politi, Y., Metzler, R. A., Abrecht, M., Gilbert, B., Wilt, F. H., Sagi, I., Addadi, L., Weiner, S. & Gilbert, P. (2008). *Proc. Natl. Acad. Sci. USA*, **105**, 17362–17366.
Ravel, B. & Newville, M. (2005). *J. Synchrotron Rad.* **12**, 537–541.
Schumacher, M., Christl, I., Scheinost, A. C., Jacobsen, C. & Kretzschmar, R. (2005). *Environ. Sci. Technol.* **39**, 9094–9100.
Skinner, A. J., LaFemina, J. P. & Jansen, H. J. F. (1994). *Am. Mineral.* **79**, 205–214.
Stöhr, J. (1992). *NEXAFS Spectroscopy*. Berlin: Springer-Verlag.
Takahama, S., Gilardoni, S., Russell, L. M. & Kilcoyne, A. L. D. (2007). *Atmos. Environ.* **41**, 9435–9451.
Toner, B., Fakra, S., Villalobos, M., Warwick, T. & Sposito, G. (2005). *Appl. Environ. Microbiol.* **71**, 1300–1310.
Urquhart, S. G. & Ade, H. (2002). *J. Phys. Chem. B*, **106**, 8531–8538.
Watts, B. & Ade, H. (2008). *J. Electron Spectrosc. Relat. Phenom.* **162**, 49–55.
Winn, B. *et al.* (2000). *J. Synchrotron Rad.* **7**, 395–404.
Zhou, D., Metzler, R. A., Tyliszczak, T., Guo, J. H., Abrecht, M., Coppersmith, S. N. & Gilbert, P. (2008). *J. Phys. Chem. B*, **112**, 13128–13135.